Topographic Axes of Wiring Space Converge to Genetic Topography in Shaping Human Cortical Layout

Deying Li,[1,2] Yufan Wang,[1,2] Liang Ma,[1,2] Yaping Wang,[1,3] Luqi Cheng,[4,5] Yinan Liu, [1,2] Weiyang Shi,[1] Yuheng Lu,[1,2] Haiyan Wang,[1] Chaohong Gao,[1,3] Camilla T. Erichsen,[6] Yu Zhang,[5] Zhengyi Yang,[1,2,3] Simon B Eickhoff,[7,8] Chi-Hua Chen,[9] Tianzi Jiang,[1,2,3,10] Congying Chu,[1*] Lingzhong Fan[1,2,3,11*]

[1] Brainnetome Center, Institute of Automation, Chinese Academy of Sciences, Beijing 100190, China

[2] School of Artificial Intelligence, University of Chinese Academy of Sciences, Beijing 100049, China

[3] Sino-Danish College, University of Chinese Academy of Sciences, Beijing 100190, China

[4] School of Life and Environmental Sciences, Guilin University of Electronic Technology, Guilin 541004, China

[5] Zhejiang Lab, Hangzhou 311121, China

[6] Core Center for Molecular Morphology, Section for Stereology and Microscopy, Department of Clinical Medicine, Aarhus University, Aarhus 8000, Denmark

[7] Institute of Neuroscience and Medicine (INM-7: Brain and Behaviour), Research Centre Jülich, Jülich 52425, Germany

[8] Institute of Systems Neuroscience, Heinrich Heine University Düsseldorf, Düsseldorf 40225, Germany

[9] Department of Radiology, University of California San Diego, La Jolla, CA 92093, USA

[10] Xiaoxiang Institute for Brain Health and Yongzhou Central Hospital, Yongzhou 425000, China

[11] School of Life Sciences and Health, University of Health and Rehabilitation Sciences, Qingdao 266000, China

*__Corresponding Authors__:

Lingzhong Fan, Institute of Automation, Chinese Academy of Sciences, Beijing 100190, China. Email: lingzhong.fan@ia.ac.cn, Phone: 010 -8254 4523

or Congying Chu, Institute of Automation, Chinese Academy of Sciences, Beijing 100190, China. Email: congying.chu@ia.ac.cn, Phone: 010 -8254 4770

Number of figures: 6

Number of extended data figures: 15

Number of extended data tables: 2

Words: abstract (250), introduction (757), discussion (1446)

Declaration of interests

The authors declare no competing interests.

Acknowledgments

This work was partially supported by STI2030-Major Projects (Grant No. 2021ZD0200200), the Natural Science Foundation of China (Grant Nos. 82072099, 82202253, 62250058), and the China Postdoctoral Science Foundation (2022M722915). Data were provided in part by the Human Connectome Project, WU-Minn Consortium (Principal Investigators: David Van Essen and Kamil Ugurbil; 1U54MH091657) funded by the 16 NIH Institutes and Centers that support the NIH Blueprint for Neuroscience Research; and by the McDonnell Center for Systems Neuroscience at Washington University. The authors appreciate the English language and editing assistance of Rhoda E. and Edmund F. Perozzi, PhDs.

Abstract

Genetic information is involved in the gradual emergence of cortical areas since the neural tube begins to form, shaping the heterogeneous functions of neural circuits in the human brain. Informed by invasive tract-tracing measurements, the cortex exhibits marked interareal variation in connectivity profiles, revealing the heterogeneity across cortical areas. However, it remains unclear about the organizing principles possibly shared by genetics and cortical wiring to manifest the spatial heterogeneity across cortex. Instead of considering a complex one-to-one mapping between genetic coding and interareal connectivity, we hypothesized the existence of a more efficient way that the organizing principles are embedded in genetic profiles to underpin the cortical wiring space. Leveraging vertex-wise tractography in diffusion-weighted MRI, we derived the global connectopies in both female and male to reliably index the organizing principles of interareal connectivity variation in a low-dimensional space, which captured three dominant topographic patterns along the dorsoventral, rostrocaudal, and mediolateral axes of the cortex. More importantly, we demonstrated that the global connectopies converge with the gradients of a vertex-by-vertex genetic correlation matrix on the phenotype of cortical morphology and the cortex-wide spatiomolecular gradients. By diving into the genetic profiles, we found that the critical role of genes scaffolding the global connectopies was related to brain morphogenesis and enriched in radial glial cells before birth and excitatory neurons after birth. Taken together, our findings demonstrated the existence of a genetically determined space that encodes the interareal connectivity

variation, which may give new insights into the links between cortical connections and arealization.

Keywords： global connectopy, genetic topography, diffusion MRI tractography, structural connectivity, cerebral cortex

Significance Statement

Genetic factors have involved the gradual emergence of cortical areas since the neural tube begins to form, shaping the specialization of neural circuitry in the human brain. However, the mechanisms through which genetics encode the complex interareal connectivity remain a pivotal and unanswered question in the field of neuroscience. Here, we hypothesized that a genetically determined space encoding the interareal connectivity variation exists, which may give new insights into the links between cortical connections and arealization. We combined diffusion tractography with a dimension reduction framework to unravel the underlying global topographic principle revealed by the anatomical connections.

Introduction

Mounting evidence has suggested that the genetic effects on the anatomical phenotypes of the human brain are spatially heterogeneous (Chen et al., 2011; Chen et al., 2012; Chen et al., 2013; Huang et al., 2023), demonstrating the vital roles of genes in establishing the configuration of brain space, such as the anatomical hierarchy (Burt et al., 2018; Wang et al., 2024) and the wiring diagram (Srinivasan et al., 2012; Greig et al., 2013; Molnar et al., 2019). The profile of cortical wiring that can be characterized using neuroimaging-based tractography is especially reliable for indicating the heterogeneity across cortical areas (Passingham et al., 2002; Fan et al., 2016; Cheng et al., 2021), reflecting differentiation in local microstructures and connectivity patterns. The interareal connectivity variation has further revealed the spatially heterogeneous patterns of cortical organization, such as regional controllability related to cognitive dynamics (Gu et al., 2015; Cui et al., 2020). In contrast, the deficit in interareal connectivity has demonstrated the specificity of the behavioral manifestations of brain lesions (Thiebaut de Schotten et al., 2020; Talozzi et al., 2023). Although spatial heterogeneity has been separately found to be embedded in genetic architecture and interareal connectivity variation, it is still largely unknown if a unified organizing principle exists underlying their indication of spatial heterogeneity.

The spatiotemporal distribution of genetic factors along the developing brain has been found to set the primary cues that guide the process of cortical arealization (O'Leary and Sahara, 2008; Cadwell et al., 2019). It has been pointed out that gene-

coded signaling molecules and transcriptional profiles may contribute to this guidance process, and these mechanisms may even be conserved into maturity (Hawrylycz et al., 2015; Vogel et al., 2024). Specifically, under the effect of morphogens secreted from the patterning centers, transcription factors are expressed in a graded manner and determine the areal fate and the expression of cell-surface molecules, thus determining the topographic organization of synaptic inputs and outputs (Rubenstein and Rakic, 1999; Chen et al., 2013) and directing axonal outgrowth (Chilton, 2006). Nevertheless, considering the complexity and flexibility of neural circuits, it is difficult to conceive of the existence of a one-to-one mapping between the genetic codes and the wiring patterns (Hassan and Hiesinger, 2015). Alternatively, we hypothesize that the genetic profiles distributed across the cortex may contain the organizing principles of cortical wiring (Hassan and Hiesinger, 2015). In this way, the genetic processes and the cortical wiring patterns can be systematically unified to provide a more complete understanding of the heterogeneity across the cortex. Recent advances in acquiring high-throughput transcriptomic data of the human brain (Shen et al., 2012) and large-scale twin samples (Chen et al., 2011; Chen et al., 2012) with neuroimaging data provide essential resources to test our hypothesis.

Furthermore, even if we can identify the genetic topography, it remains unknown whether we can leverage it to explain the interareal connectivity variation captured by high-resolution connectomics (Taylor et al., 2017; Mansour et al., 2021). Recent studies have revealed that cortical areas are hierarchically organized along the

cortex from a large-scale gradient perspective of connectivity (Margulies et al., 2016; Huntenburg et al., 2018), indicating that the cortex is organized topologically within interareal connectivity variation, supporting diverse dynamics and functions (Atasoy et al., 2016; Robinson et al., 2016; Preti and Van De Ville, 2019; Chu et al., 2024). However, traditional neural circuit tracing techniques, including classical tracers or virus tracing, are precluded in humans, thereby creating the need for noninvasive measures of the topography embedded in interareal connectivity variation, which could contribute to testing the existence of unified rules underlying the genetic topography and interareal connectivity variation.

To address these open questions, we first quantified the interareal connectivity variation by establishing the similarity matrix of the structural connectivity profiles. Leveraging a manifold learning approach, we identified three components (hereafter also referred to as global connectopy) running separately along the dorsoventral, rostrocaudal, and mediolateral axes of the brain anatomy, which efficiently delineated the interareal connectivity variation. Then, we characterized the genetic topography by respectively utilizing the gradients from the twin-based genetic correlation matrix of cortical morphology and the cortex-wide gene expression matrix. Based on the identified global connectopy and the genetic topography, we provided evidence supporting our hypothesis by demonstrating the significant consistency between them. Furthermore, we identified specific genes associated with the global connectopies that were involved in brain morphogenesis and enriched in radial glial cells before birth and excitatory neurons related with cortical projection circuit

157 formation after birth. Our analytic logic is detailed in Figure 1 to provide an overview

158 of the current study.

159

Materials and Methods

Data and preprocessing

Data collection We used a publicly available dataset containing 100 unrelated subjects (HCP-U100) (46 males; mean age, 29.11±3.67; age range, 22-36) provided by the Human Connectome Project (HCP) database (Van Essen et al., 2013) (http://www.humanconnectome.org/). All the scans and data from the individuals included in the study had passed the HCP quality control and assurance standards.

The scanning procedures and acquisition parameters were detailed in previous publications (Glasser et al., 2013). In brief, T1w images were acquired with a 3D MPRAGE sequence on a Siemens 3T Skyra scanner equipped with a 32-channel head coil with the following parameters: TR = 2400 ms, TE = 2.14 ms, flip angle = 8°, FOV = 224×320 mm^2, voxel size = 0.7 mm isotropic. Diffusion data were acquired using single-shot 2D spin-echo multiband echo planar imaging on a Siemens 3 Tesla Skyra system (TR = 5520 ms, TE = 89.5 ms, flip angle = 78°, FOV = 210×180 mm). These consisted of three shells (b-values = 1000, 2000, and 3000 s/mm^2), with 90 diffusion directions isotropically distributed among each shell and six b = 0 acquisitions within each shell, with a spatial resolution of 1.25 mm isotropic voxels.

Image preprocessing The human T1w structural data had been preprocessed following the HCP's minimal preprocessing pipeline (Glasser et al., 2013). In brief, the processing pipeline included imaging alignment to standard volume space using FSL, automatic anatomical surface reconstruction using FreeSurfer, and registration

to a group average surface template space using the multi-modal surface matching (MSM) algorithm (Robinson et al., 2014). Human volume data were registered to the Montreal Neurological Institute (MNI) standard space, and surface data were transformed into surface template space (fs_LR).

The diffusion Images were processed using FDT (FMRIB's Diffusion Toolbox) of FSL. The main steps included normalization of the b0 image intensity across runs and correction for echo-planar imaging (EPI) susceptibility, eddy-current-induced distortions, gradient-nonlinearities, and subject motion. DTIFIT was then used to fit a diffusion tensor model. The probability distributions of the fiber orientation distribution were estimated using Bedpostx.

Next, skull-stripped T1-weighted images for each subject were co-registered to the subject's b0 images using FSL's FLIRT algorithm. Then, nonlinear transformations between the T1 image and the MNI structural template were obtained using FSL's FNIRT. By concatenating these, we derived bi-directional transformations between the diffusion and MNI spaces.

Connectopy mapping

Tractography and connectivity blueprints To map the whole-brain connectivity pattern, we performed probabilistic tractography using FSL's probtrackx2 accelerated by using GPUs (Behrens et al., 2007; Hernandez-Fernandez et al., 2019). Specifically, the white surface was set as a seed region tracking to the rest of the brain with the ventricles removed and down-sampled to 3 mm resolution. The pial

surface was used as a stop mask to prevent streamlines from crossing sulci. Each vertex was sampled 5,000 times (5,000 trackings) based on the orientation probability model for each voxel, with a curvature threshold of 0.2, a step length of 0.5 mm, and a number of steps of 3,200. This resulted in a (*whole-surface vertices*) × (*whole-brain voxels*) matrix for further analysis. We checked the preprocessing images and tractography results of each subject to ensure the accuracy of our analysis. Specifically, the reconstructed surfaces were visually inspected, and transforms between different spaces were checked carefully. Tractography results were also visually checked to ensure that no streamlines crossed the sulci. We also calculated whole-brain connections at the ROI-wise. We performed tractography from regions to the whole brain using Schaefer-400 parcellation (Schaefer400) (Schaefer et al., 2018) to get a *(whole brain ROIs)* × (*whole-brain voxels*) matrix for further analysis.

We additionally created connectivity blueprints following previous work (Mars et al., 2018), which had been used to characterize connectivity patterns of brain regions or cortical vertices. Specifically, we first reconstructed 72 fiber bundles using a pre-trained deep-learning model, TractSeg (Wasserthal et al., 2018), and down-sampled the resulting tract masks to 3 mm resolution, yielding a (*tracts*) × (*whole-brain voxels*) matrix. The connectivity blueprints were then generated by the product of this tract matrix and the whole-brain connectivity matrix, which was obtained and normalized as described in the Tractography section. The columns of the resulting (*tracts*) ×

(*whole-surface vertices*) matrix showed the connectivity distribution pattern of each cortical vertex, while the rows revealed the cortical termination patterns of the tracts.

Tractogram covariance analysis We calculated the tractogram covariance (TC) matrix to characterize the structural connectivity similarity profile. The vertex profiles underwent pairwise Pearson correlations, controlling for the average whole-cortex profile. For a given pair of vertices, *i* and *j,* TC was calculated as

$$TC(i,j) = \frac{r_{ij} - r_{ic}r_{jc}}{\sqrt{(1 - r_{ic}^2)(1 - r_{jc}^2)}}$$

in which r_{ij} was the Pearson correlation coefficient of the structural connectivity profile at vertices *i* and *j*, r_{ic} the correlation of the structural connectivity profile at vertex *i* with the average connectivity profile across the whole cortex, and r_{jc} the correlation of the structural connectivity profile at vertex *j* with the average connectivity profile across the entire cortex. A symmetric ~30k × 30k TC matrix was produced for each subject. The TC matrices of all subjects were then averaged separately for the left and right hemispheres to obtain a group-level TC matrix for each hemisphere. In line with a previous study (Paquola et al., 2019), the TC matrix was proportionally thresholded at 90% per row, with elements above zero retained to remove negative connections.

Connectopy decomposition The TC matrix was transformed into a non-negative square symmetric affinity matrix using a cosine affinity kernel. Then, diffusion map embedding was implemented to identify the principal gradient components (Coifman et al., 2006). Diffusion map embedding is a nonlinear manifold learning technique

that maps cortical gradients (Margulies et al., 2016). Along these gradients, cortical vertices with similar connectivity profiles are embedded along the axis. Diffusion map embedding is relatively robust to noise and less computationally expensive than other nonlinear manifold learning techniques.

Global connectopies were computed separately for the left and right hemispheres with two key parameters: α controls the influence of the density of sampling points on the manifold, and t controls the scale of the eigenvalues. Here, we set α=0.5 and t=0 as recommended (Margulies et al., 2016). The amount of explained variance was assessed, and the first three global connectopies were chosen to map onto the cortical surface for further analysis. The ROI-wise global connectopies were also computed in the same model.

Individual global connectopies were calculated for each subject and aligned to the group GC with Procrustes rotation, which matches the order and direction of the global connectopies without scaling. The application of Procrustes rotation allows for comparison between individuals.

Projection of the global connectopies onto the white matter voxels We used general linear models (GLM) to project the global connectopies onto the white matter (Tarun et al., 2020), exploring the contribution of each white matter voxel to the global connectopies. Specifically, we used the global connectopies as the dependent variable and the structural connection matrix as the independent variable. The resultant weights indicate the contribution of each white matter voxel. Note that the

structural connection of each subject was obtained from probabilistic tractography in individual diffusion space. Each subject's data were registered to MNI standard space and averaged, resulting in a group-level structural connection matrix.

Projection of the connectopies onto the white matter tracts To investigate how the global connectopies are related to the underlying white matter tracts, we created a tract projection map using the tract mask generated by TractSeg. Seventy-two tracts identified by TractSeg were grouped into five types for analysis: association tracts, commissural tracts, projection tracts, thalamo tracts, and striato tracts (Table S2-1). Using the connectivity blueprints we built earlier, we extracted the projection on the surface of each tract and calculated the mean value and variance using the connectopy values of tract projection on the surface, thus revealing the relationship between the tracts and global connectopies. Due to the absence of projection on the surface, we excluded the fornix (FX), superior cerebellar peduncle (SCP), middle cerebellar peduncle (MCP), and inferior cerebellar peduncle (ICP) from the study. We additionally removed the Corpus Callosum – all because several of its segments were also reconstructed by TractSeg, i.e., CC_1 to CC_7.

Visualization of connectopies To intuitively inspect the global connectopies together, we plotted every pair of global connectopies in a 2D space and assigned colors based on their positions. Then, we generated RGB values for each vertex by normalizing the three global connectopy values and mapped them on the surface, showing the dominant global connectopy at the vertex. Specifically, for the first

gradient, the values of all vertices were normalized from zero to one, resulting in the value of the red channel. The other two were conducted the same.

Hierarchical organization analysis

We implemented hierarchical clustering using global connectopies to test if the global connectopies could provide a descriptor of arealization. At the first level, the vertices were sorted in descending order based on the first global connectopy. Brain regions were partitioned into two subregions according to the sign of the connectopy value. Furthermore, based on the positivity and negativity of the second and third global connectopies, the whole cortex was partitioned into eight modules.

Gene analysis

Genetic correlation analysis of thickness and surface area We selected 194 twins from the HCP database (102 monozygotic and 92 dizygotic pairs; mean age, 29.96±2.96; age range, 22-36). The cortical surface was reconstructed to measure cortical thickness and surface areas at each surface location using FreeSurfer in the fsaverage3 template to reduce computation time.

In a classical twin study of sets of monozygotic (MZ) and dizygotic (DZ) twins, four latent factors could account for the variance of any phenotype: additive genetic effects (A); non-additive genetic effects, including dominance (D); common or shared environmental effects (C); and non-shared or individual-specific environmental effects (E). Since MZ twins are assumed to be genetically identical, their genetic correlation is perfect (r = 1.0) for both additive and non-additive genetic effects. In

307 contrast, DZ twins share, on average, 50% of their genes, resulting in correlations of
308 0.50 for additive genetic effects and 0.25 for non-additive genetic effects. The C term
309 refers to environmental factors that contribute to similarities between twins; thus,
310 shared environmental factors have a correlation of 1.0 across twin pairs, regardless
311 of zygosity. The E term represents environmental factors that create differences
312 between twins. Since these are individual-specific factors, they are considered
313 uncorrelated across twins.

314 Given the minimal difference between the A and D effects, we fitted bivariate
315 ACE models to calculate the genetic correlations of cortical thickness and surface
316 area between two cortical vertices. This approach allows us to explore both genetic
317 and environmental contributions to variance and covariance. A phenotypic correlation
318 reflects the shared variance between two traits, combining both genetic and
319 environmental components. Specifically, it is defined as the total covariance (genetic
320 plus environmental) between two variables, divided by the square root of the product
321 of their respective total variances. After decomposing variance sources in the
322 bivariate model, we computed genetic correlations, which represent the genetic
323 covariance divided by the square root of the product of the genetic variances of the
324 two variables. The analyses were performed using OpenMx (Neale et al., 2016). The
325 terms of the output genetic correlation matrix represented the genetic correlation
326 decomposed from the total phenotypic correlation between two cortical vertices.

327 We then implemented diffusion map embedding on the genetic correlation matrix
328 and compared it with the global connectopies. Genetic patterning results were

obtained from previous studies (Chen et al., 2012; Chen et al., 2013), which parcellated the cortex into four and twelve clusters. The parcellation results were compared with the modules derived from hierarchical clustering using the global connectopies.

AHBA data and preprocessing Regional microarray gene expression data were obtained from 6 postmortem brains (1 female, ages 24-57) provided by the Allen Human Brain Atlas (AHBA, https://human.brain-map.org/). The data were processed using the abagen toolbox (version 0.1.1; https://github.com/rmarkello/abagen) (Markello et al., 2021). First, the microarray probes were reannotated (Arnatkeviciute et al., 2019), and probes that did not match a valid Entrez ID were excluded. Then, the probes were filtered based on their expression intensity relative to background noise, and the probes with the maximum summed adjacency for representing the corresponding gene expression were kept, yielding 15,633 genes corresponding to more than one probe. Finally, we resampled the output gene expression map in fs5 space to fsaverage_LR32k space for subsequent study.

Analysis of morphogen gradient-related genes We further selected morphogen genes in AHBA data (Rakic et al., 2009) and examined their expression difference along the global connectopies. Each global connectopy was subdivided equally into ten parts, and two sample t-tests were used to assess the difference in gene expression of selected genes between the first and the last bins (Fjell et al., 2019). We also examined the differential stability (DS) of morphogen genes, which is defined as the tendency for a gene to exhibit reproducible differential expression

relationships across brain structures, specifically the average Pearson correlation over 15 pairs of 6 brains in the AHBA dataset (Hawrylycz et al., 2015).

Correspondence to spatiomolecular gradients Researchers recently reported three spatiomolecular gradients that retained the same pattern as morphogenetic gradients during development, which varied along three spatially embedded axes (Vogel et al., 2024). We only used data from the left hemisphere to reproduce these molecular gradients follow the previous publication, because few samples in the AHBA were obtained from the right hemisphere.

Gene enrichment analysis We used a prediction framework, partial least squares regression (PLSR), to determine the covariance between gene expression and global connectopies. We then conducted 1,000 bootstrapping to estimate the error of the weight of each gene. The normalized weight of each gene was denoted as the weight divided by the estimated error (Morgan et al., 2019).

Genes were selected as the top and bottom 0.83% genes (n = 260) of each global connectopy's gene list, corrected for both tails and all three global connectopies for multiple comparisons. Each gene set, combining both tails, underwent cell-type enrichment analysis on the filtered genes using CellGO (http://www.cellgo.world) (Li et al., 2023). Single-cell datasets collected from prenatal (Fan et al., 2020) and postnatal sample were used (Ma et al., 2022). Seven major classes of cells were provided in the prenatal sample, including radial glial cells (RG), intermediate progenitor cells (IPC), excitatory neurons (ExN), inhibitory neurons

(InN), oligodendrocyte precursor cells/oligodendrocytes (OPC/Oligo), astrocytes (Astro), and microglia cells (Microglia). Six major classes of cells were provided in the postnatal sample, including ExN, InN, Oligo, OPC, Astro, and Microglia. The enrichment *P*-values of the cell types resulting from the submitted genes were based on the Kolmogorov-Smirnov (K-S) test in CellGO.

We collected gene expression data for all time points in the BrainSpan dataset to determine the developmental pattern of gene expression (Miller et al., 2014). Only genes associated with all three global connectopies were selected. Non-negative matrix factorization was used to derive the gene expression components for each macrostructure in the brain.

The filtered genes extending across the three global connectopies were also submitted to gene ontology enrichment analysis. ToppGene (https://toppgene.cchmc.org/), which contains the complete list of AHBA genes as the background gene set, was used to conduct the analysis. The following term categories were assessed: GO: Molecular Function, GO: Biological Process, GO: Cellular Component, Pathway, and Disease.

Replication and robustness analyses

Replication with CHCP dataset We randomly selected 100 age-matched subjects (59 males; mean age, 24.31±2.35; age range, 22-35) from the Chinese Human Connectome Project (CHCP) dataset (Ge et al., 2023). All subjects provided written

informed consent, and the protocol was approved by the Institutional Review Board at Peking University.

The scanning procedures and acquisition parameters were detailed in previous publications (Ge et al., 2023). In brief, T1w images were acquired on a 3T Siemens Prisma scanner with the following parameters: TR = 2400 ms, TE = 2.22 ms, flip angle = 8°, FOV = 256×240 mm2, voxel size = 0.8 mm isotropic. Diffusion data were acquired with the following parameters: TR = 3500 ms, TE = 86 ms, flip angle = 90°, FOV = 210×210 mm), voxel size = 1.5 mm isotropic, 14 baseline images at b = 0, 93 diffusion-weighted images at b = 1000 s/mm^2, and 92 diffusion-weighted images at b = 2000 s/mm^2.

The structural and diffusion data from the CHCP dataset were preprocessed with HCP's minimal preprocessing pipeline (Glasser et al., 2013), which was consistent with the HCP dataset. We repeated the procedure of construction of global connectopies on the CHCP dataset and compared the similarity with GCs in the HCP dataset.

Examine the confound effect Complementing our main analysis on calculating global connectopies, we examined the effect that may be caused by age, sex, and brain size. For age, we divided subjects into three groups (age 20-25: *n* = 17; age 25-30: *n* = 40; age 30-35: *n* = 43). For sex, we divided the subjects into males (*n* = 46) and females (*n* = 54). For brain size, we extracted each HCP subject's total intracranial volume (TIV) from the FreeSurfer output. Moreover, we divided into five groups (TIV 1.0-1.2: *n* = 3; TIV 1.2-1.4: *n* = 12; TIV 1.4-1.6: *n* = 38; TIV 1.6-1.8: *n* =

40; TIV 1.8-2.0: *n* = 7; [*10^6 mm3]). We calculated the correlation of the tractogram covariance matrix between groups.

Examine the distance and geometry effect. We derived the geodesic distance matrices on the mid-thickness surface of the human brain, calculated the gradients, and computed the correlation with global connectopies to test the effect of geodesic distance. We also remove short-range connections in the tractogram covariance matrices. We removed the value if the geodesic distance of the two vertices was less than 10mm, 20mm, and 30mm, respectively, and calculated the global connectopies again.

We further followed the procedure from a previous study to obtain the cortical geometric eigenmodes (Pang et al., 2023). In brief, because the brain structure can be approximated as being constant in time, the resulting spatial and temporal dynamics can be treated separately via eigenmode decomposition. In particular, the spatial aspect satisfies the Laplacian eigenvalue problem, which is also known as the Helmholtz equation, defined in the following equation,

$$\Delta := \frac{1}{W}\sum_{i,j}\frac{\partial}{\partial x_i}\left(g^{ij}W\frac{\partial}{\partial x_j}\right)$$

where x_i, x_i are the local coordinates, g^{ij} is the inverse of the inner product metric tensor $g_{ij} := <\frac{\partial}{\partial x_i}, \frac{\partial}{\partial x_i}>$, $W := \sqrt{\det(G)}$, det denoted the determinant, and $G := (g_{ij})$.

We derived the geometric eigenmodes of the cortical surfaces by solving the eigen-decomposition problem $\Delta U = U\Lambda$, where U is composed of eigenvectors

435 $u_i$and the corresponding eigenvalue λ_i. Specifically, we used a triangular surface
436 mesh representation of the gray-white matter interface cortical surface, comprising
437 32,492 vertices in each hemisphere. The surface used for the HCP analysis was
438 from the published version
439 (https://github.com/ThomasYeoLab/CBIG/tree/master/data/templates/surface/fs_LR_
440 32k). Since the first eigenmode presents a constant pattern on the surface, we
441 compared the following geometric eigenmodes with three GCs.
442

Results

Three global connectopies in the human brain

To explore how the spatial organization of the human brain is shaped by the underlying structural connections within the white matter, we characterized the global connectopies across the whole brain. We first built a vertex-wise similarity matrix of structural connectivity using 100 unrelated subjects from the Human Connectome Project dataset (Van Essen et al., 2013). Specifically, structural connectivity profiles were obtained from probabilistic tractography along approximately 30k vertices for each hemisphere and were correlated between each pair of vertices. Tractogram covariance (TC) matrices were thresholded at 0 and averaged across subjects. In short, the TC matrix captured structural connectivity similarity across the whole brain.

We implemented diffusion embedding on the TC matrix, a manifold learning method previously used to capture functional gradients (Coifman et al., 2006). The resultant components revealed the position of vertices along the axes with the most dominant differences in the given structural connectivity profile. The first three global connectopies separately showed dorsoventral, rostrocaudal, and mediolateral patterns and together accounted for 33% of the total variance (Figure 2a).

More specifically, the first global connectopy (Global connectopy 1 dorsoventral, GC1-DV), following a dorsoventral pattern, was anchored at one end by the occipital, inferior temporal, and orbitofrontal cortex and at the other end by the sensorimotor cortex. The second global connectopy (Global connectopy 2 rostrocaudal, GC2-RC)

varied along a rostrocaudal axis, radiating from the occipitoparietal cortex and ending in the prefrontal cortex. The third global connectopy (Global connectopy 3 mediolateral, GC3-ML) showed a mediolateral pattern, with the highest expression in the lateral temporal and prefrontal cortex and the lowest in the cingulate cortex (Figure 2a).

These patterns were stable regardless of the number of subjects considered (Figure 2-1) and were not affected by age, sex, or brain size (Figure 2-2). The findings were consistent in a replication sample from the Chinese Human Connectome Project dataset (n = 100; Figure 2-3) (Ge et al., 2023). Individual global connectopies were computed for each subject and aligned to the group GC with Procrustes rotation, allowing for individual comparison. The individual GCs were highly correlated with the group GC (all r > 0.9; Figure 2-4). To reduce the influence of noise, we used Schaefer-400 parcellation (Schaefer et al., 2018) to calculate ROI-wise global connectopies. The results showed that the first three gradients corresponded to the three vertex-wise global connectopies (Figure 2-5). We further showed that global connectopies are beyond geodesic distance and cortical geometry (Figure S2-6, 2-7) and demonstrated the role of long-range connections in the formation of global connectopies (Figure 2-8). These results showed that global connectopies were not simply the result of spatial autocorrelation.

The three connectopies are situated by distinct sets of white matter tracts

We further explored how the underlying white matter shaped these spatial organizations. We fitted general linear models (GLMs) to interpolate measures from the gray matter into the white matter (Tarun et al., 2020). Specifically, we used the global connectopies as the dependent variable and the structural connection matrix as the independent variable, thus projecting each global connectopy onto the white matter (Figure 2-9). For GC1-DV, the white matter voxels were distributed along the dorsal-ventral axis beneath the surface. Specifically, voxels near the sensorimotor cortex and occipitotemporal cortex showed values that were markedly consistent with the locations of the extremes of the first global connectopy. Voxels corresponding to GC2-RC and GC3-ML varied from posterior to anterior and medial to lateral.

We then focused on the specific tracts related to the emergence of the global connectopies. We reconstructed 72 fiber bundles following TractSeg (Wasserthal et al., 2018) (Table 2-1) and built group-level connectivity blueprints (Mars et al., 2018), where the rows revealed the cortical termination patterns of the tracts. We first extracted the projection on the surface of each tract and calculated the mean value and variance of connectopy values of the tract projection on the surface (Figure 2b). We identified the tracts that were either situated at one of the extremes of the global connectopy or were spread out along the axis. The results for the bilateral tracts were averaged between the two hemispheres and are shown in the scatterplot (Figure 2b; detailed values are shown in Figure 2-10).

Two types of characteristic tracts are shown in the right columns of Figure 2b, including the thalamo-precentral tract (T_PREC), striato-occipital tract (ST_OCC), and thalamo-parietal tract (T_PAR) for GC1-DV as well as the middle longitudinal fascicle (MLF), thalamo-prefrontal tract (T_PREF), superior longitudinal fascicle II (SLF_II) for GC2-RC, along with the arcuate fascicle (AF), cingulum (CG), and MLF for GC3-ML.

For GC1-DV, T_PREC, which connects the thalamus with the precentral gyrus, is related to motor task performance (Strick, 1986). T_PREC has a distinctly vertical expanding shape and showed high mean values near the dorsal end of GC1-DV, expressing the most significant contribution to the global connectopy. ST_OCC connects the striatum with the occipital cortex, showing high mean values at the ventral end and having a "stretching" impact on the global connectopy pattern. In contrast, T_PAR has a high variance within GC1-DV and appears to constrain the global connectopy formation.

For GC2-RC, the second branch of the superior longitudinal fascicle, which mostly runs from the posterior to the anterior, starting from the middle frontal gyrus and terminating in the angular gyrus, had the greatest mean value for the white matter tract. The SLF_II, which covered most of the areas in the second global connectopy, also showed high values, providing the prefrontal cortex with parietal cortex information about the perception of visual space and providing information about working memory in the prefrontal cortex to the parietal cortex to focus spatial attention and regulate the selection of spatial information (Janelle et al., 2022). Other

"high-contribution" tracts, including the MLF and T_PREF, are located either in the anterior or posterior regions.

The GC3-ML showed a similar pattern to the tracts that made high contributions. The corpus callosum, the giant white matter fiber bundle consisting of millions of axonal projections, spans from the medial brain through different parts of the cortex and connects all the brain lobes. Thalamo- and striato-cortical projections also extend from the subcortical nuclei to reach different lateral cortices. We suggest that the former type of tract plays a role in stretching the brain along the axis, while the latter type has a constraining effect, and that these work together to shape the organization of the brain.

Global connectopies provide a large-scale descriptor of arealization

To inspect the global connectopies as a unit, we normalized three connectopy values at each vertex to generate RGB values and mapped them on the surface to make lobes or subregions visible distinctly (Figure 3a). We termed this map the global connectopic space, which quantified the topography of the dominant global connectopy. The cortex, shown in red, green, and blue, indicates the individual regions dominated by each global connectopy. Regions dominated by a combination of more than one global connectopy were represented in different colors, e.g., the "yellow" region was dominated by the first and second global connectopies together, as shown in the cube in Figure 3a.

We then plotted every pair of global connectopies in a 2D space and assigned colors based on the global connectopic space in Figure 3a. The first and second global connectopies interacted to split the whole brain into the prefrontal cortex and limbic cortex, sensorimotor cortex, and occipitotemporal cortex (Figure 3b). Similarly, the frontal cortex, limbic cortex, and occipitotemporal cortex were shown when the first and third global connectopies were considered together (Figure 3b). The prefrontal cortex, limbic cortex, and others were shown when the second and third connectopies were combined (Figure 3b). The three GCs were also plotted together in 3D space, with vertices assigned different colors according to the signs of the three axes (Figure 3b, right).

In order to show the modules clearly in the global connectopic space, we partitioned the brain by hierarchical clustering using the three global connectopies (Figure 3c). At the first level, the brain was partitioned into two modules based on the positive and negative signs of the first global connectopy. These two modules coincided with the division between the dorsal and ventral brain regions. Each module was further partitioned into two modules at each level by the sign of the global connectopies. The rostrocaudal and mediolateral patterns emerged after considering the corresponding global connectopy. In the end, eight modules were captured: the ventral and dorsal somatomotor cortex, lateral prefrontal cortex, cingulate gyrus, lateral temporal cortex + angular gyrus, medial occipital cortex + occipital polar cortex, orbitofrontal cortex, and ventromedial prefrontal cortex + posterior cingulate cortex (Figure 3c). Note that the parcellation guided by the three

global connectopies is very coarse compared with several fine-grained brain atlases that have been delineated using the gradient approach (Gordon et al., 2016; Schaefer et al., 2018). We did not utilize these more fine-grained parcels because we believe they are more likely to be shaped by local gradients compared with the three global connectopies, which characterize the global pattern across the brain.

Potential genetic basis underlying global connectopies

Having established the global connectopies in the human brain, we first explored the relationship between the genetic influence on cortical morphology and the identified global connectopies. We estimated the pairwise genetic correlation between vertices on the cortex by fitting a bivariate ACE model, which revealed shared genetic influences on cortical thickness and relative area expansion between cortical vertices. The resultant genetic correlation matrix represented the genetic correlation decomposed from the total phenotypic correlation between the two cortical vertices. The first three gradients decomposed from the genetic correlation matrix of cortical thickness showed a rostral-caudal axis, a medial-lateral axis, and a dorsal-ventral axis, respectively (left: $r_{GC1\text{-}DV,\ GG3\text{-}Thickness} = 0.72$, $p_{spin} < .0028$, FDR corrected; $r_{GC2\text{-}RC,\ GG1\text{-}Thickness} = 0.91$, $p_{spin} < .0001$, FDR corrected; $r_{GC3\text{-}ML,\ GG2\text{-}Thickness} = 0.72$, $p_{spin} < .0041$, FDR corrected; right: $r_{GC1\text{-}DV,\ GG3\text{-}Thickness} = 0.73$, $p_{spin} < .0044$, FDR corrected; $r_{GC2\text{-}RC,\ GG1\text{-}Thickness} = 0.88$, $p_{spin} < .0098$, FDR corrected; $r_{GC3\text{-}ML,\ GG2\text{-}Thickness} = 0.71$, $p_{spin} < .1566$, FDR corrected; Figure 4a, 4b). The first three gradients decomposed from the genetic correlation matrix of the surface area correspond with the three global connectopies (left: $r_{GC1\text{-}DV,\ GG1\text{-}Area} = 0.53$, $p_{spin} < .1630$; $r_{GC2\text{-}RC,\ GG2\text{-}Area} = 0.49$, $p_{spin} <$

590 .0006, FDR corrected; $r_{GC3\text{-}ML,\ GG3\text{-}\ Area}$ = 0.51, p_{spin} < .1031; right: $r_{GC1\text{-}DV,\ GG1\text{-}Area}$ = 0.58,
591 p_{spin} < .2131; $r_{GC2\text{-}RC,\ GG2\text{-}\ Area}$ = 0.46, p_{spin} < .0177; $r_{GC3\text{-}ML,\ GG3\text{-}\ Area}$ = 0.51, p_{spin} < .0812;
592 Figure 4-1). We replicated the global connectopies using twin data from the HCP and
593 found they show high similarity with the results derived from unrelated subjects (left:
594 $r_{G1\text{-}DV}$ = 0.99, $r_{G2\text{-}RC}$ = 0.99, $r_{G3\text{-}ML}$ = 0.99; right: $r_{G1\text{-}DV}$ = 0.99, $r_{G2\text{-}RC}$ = 0.98, $r_{G3\text{-}ML}$ = 0.98;
595 Figure 4-2). Each parcel derived from the fuzzy clustering of the genetic correlation
596 matrix of cortical thickness (Chen et al., 2012) also showed significant overlap with
597 one of the four parcels derived from the hierarchical clustering identified using the
598 global connectopies (Figure 4c, Figure 4-3a, b and Figure 4-4a, b). The overlap
599 between parcels derived from the hierarchical clustering and parcels from the genetic
600 correlation of surface area is additionally shown in Figure 4-3c, d and Figure 4-4c, d.
601 These significant correspondence levels indicated a close genetic relatedness of the
602 global connectopies.

603 Since the morphogen gradients have been established and their pattern was
604 conserved during the development (Vogel et al., 2024), we explored whether these
605 genetic patterns correspond with those of the structural connectivity. We first
606 identified the morphogen genes in AHBA data according to a previous publication
607 (Rakic et al., 2009). These genes exhibited high differential stability across
608 individuals, with 80% of morphogen genes located in the top half of DS genes (Δ_{BR} >
609 0.5284; Table 5-1), suggesting their involvement in common functionality and
610 dysfunctionality in human brains (Hawrylycz et al., 2015). We subdivided the
611 connectopies equally into ten parts. Two sample t-tests were used to assess the

612 difference in gene expression of these genes between the first and the last bins. We
613 found that the expression of *FGF17* was significantly higher in the dorsal cluster than
614 in the ventral cluster (t = 27, p < .001), while the expression of *FOXG1* was
615 significantly higher in the ventral cluster (t = -25, p < .001). The same opposite
616 patterns were observed between *FGF8* (rostral < caudal, t = -33, p < .001) and *PAX6*
617 (rostral > caudal, t = 29, p < .001), and between *SFRP1* (medial < lateral, t = -41, p <
618 .001) and *WNT3* (medial > lateral, t = 99, p < .001; Figure 5a). The number of
619 subdivisions does not affect the final results (Figure 5-1).

620 The above analyses showed a genetic association with morphogen axes in the
621 developing brain. Next, we investigated whether the directional gradients of gene
622 expression in the adult human brain, i.e., spatiomolecular gradients (Vogel et al.,
623 2024), correlate with global connectopies. The spatiomolecular gradients delineated
624 the topographic variation of gene expression spanning the adult human brain and
625 were reported to capture previously identified rostral-caudal, dorsal-ventral, and
626 medial-lateral axes of early developmental patterning (Vogel et al., 2024). We
627 showed that the three global connectopies had significant correlations with the
628 spatiomolecular gradients ($r_{GC1\text{-}DV,\ LV1}$ = 0.74, p_{spin} < .0060, FDR corrected; $r_{GC2\text{-}RC,\ LV2}$
629 = 0.75, p_{spin} < .0012, FDR corrected; $r_{GC3\text{-}ML,\ LV3}$ = 0.5, p_{spin} < .0233, FDR corrected;
630 Figure 5b). Note that the gradient values for the subcortex, cerebellum, and
631 brainstem were excluded, and only data for the cortex were considered. Since the
632 LV3 gradient showed the most variation and varied along a mediolateral and
633 dorsoventral direction, as mentioned previously (Vogel et al., 2024), the r-value was

lower compared with the former two but still significant, and the correlation between the first global connectopy was also moderate ($r_{GC1\text{-}DV,\ LV3}$ = -0.36, p_{spin} < .05). These findings again suggested a potential genetic basis underlying the global connectopies.

Finally, we explored the roles of genes that contributed to the global connectopies. We used partial least squares regression (PLSR) on the AHBA data and filtered the genes with the top 5% weight for each global connectopy after 1000 times bootstrapping (corrected for multiple comparisons). We found that a selection of genes contributed to more than one global connectopy, with 22 genes overlapping with all three (Figure 6a, right). All significantly associated genes overlapped with known morphogenetic genes identified previously (Rakic et al., 2009) (hypergeometric test, p < .001; Figure 6b, right). The top genes in each global connectopy, such as *FARSA*, *MPND*, *SYCP2*, *CUX1*, *ARHGDIG*, and *NUDT14*, are known to be associated with the regulation of transcription factor activity, morphogenesis, cell proliferation, and metabolic processes (Figure 6b) (Adra et al., 1998; Yang et al., 2006; Zhu et al., 2007; Sansregret and Nepveu, 2008; Heyen et al., 2009; Arikkath, 2012; Krenke et al., 2019), while genes related to all three global connectopies, including *ADAMTSL1* and *TIAM1*, showed an obvious connection with various diseases (Figure 6b) (Hendee et al., 2017; Lu et al., 2022; Ru et al., 2022). This finding is consistent with the observation that disruptions in forming early developmental gradients through mutations to gradient-associated genes can cause severe developmental disorders (Flores-Sarnat and Sarnat, 2008; Vogel et al., 2024).

We found these genes to be significantly enriched in radial glial cells in prenatal samples (Figure 6c, left) and enriched in excitatory neurons after birth (Figure 6c, right). This was verified by the developmental pattern of these genes provided by all time points in the BrainSpan dataset (Miller et al., 2014), which showed that they were highly expressed in the prenatal period in all lobes and that their expression decreased after birth (Figure 6d), suggesting that the patterns present in adulthood were nearly established in the early stages of development. Digging deeper into specific biological processes, the gene ontology enrichment analysis showed that these genes were related to the regulation of transcription, metabolic process, morphogenesis, cellular development, and neuron projection (Figure 6e).

Discussion

In the current study, we demonstrated that a low-dimensional, topological representation of brain connectivity exists and may share common space with gene expression, despite the significant disparity in the numbers of genes and connections. We systematically analyzed the spatial topography of cerebral connectivity, i.e., the white matter tractogram, and identified three orthogonal global connectopies: the dorsoventral, rostrocaudal, and mediolateral connectopies across the cerebral cortex, which are represented in the spatial arrangement of long-range white matter tracts. Moreover, the global connectopies were observed to align with the gradients of morphogens identified during embryonic brain development and with genetic topography and spatiomolecular gradients. Our findings demonstrate the crucial role that comprehending the connectivity topographies and their genetic constraints plays in understanding the underlying principles that shape human brain organization.

The three orthogonal global connectopies derived from the white matter closely resemble the principal axes of brain development (Takahashi et al., 2012; Vogel et al., 2024) and the chemotactic gradients of early embryogenesis (Van Haastert and Devreotes, 2004; Wu, 2005). From a developmental perspective, both the encoding of chemical gradients by morphogens and the spatial expression patterns of all genes during the formation of the mature brain, along with recent research on phenotypic mapping facilitated by twin studies (Chen et al., 2011; Chen et al., 2012; Chen et al., 2013), indicate that gradient-based organizational principles may serve

689 as one of the fundamental rules in the precise formation of gene-encoded
690 connections and the establishment of functional cortical regions. Indeed, genes
691 provide the initial blueprint that guides differentiation and the directional migration of
692 neurons through the subsequent formation of different types of gradients of
693 morphogens, and, in parallel, the precise trajectory and projection of axons (Kast and
694 Levitt, 2019). Given the significant disparity in the numbers of genes and
695 connections, genes might not drive the precise details of complex circuit diagrams
696 but have the potential to influence their organizational rules by enacting pattern
697 formation rules to increase the probability that neurons make the correct connections
698 (Hassan and Hiesinger, 2015; Langen et al., 2015). This simple genetic rule may
699 underpin the global connectome organization, consistent with the argument that
700 anatomical connections could characterize the arealization and show consistency
701 with cortical patterns driven by genetic profiles (Cui et al., 2016; Fan et al., 2016;
702 Fan, 2021).

703 Interestingly, the high correspondence between modules identified using global
704 connectopies and those obtained from genetic topographies (Chen et al., 2013) may
705 also provide evidence for the role of connections in the initial scaffolding for cortical
706 organization. Previous research found that cortical patterning creates segregated
707 areas with different functions via cell differentiation and migration, specifically
708 occurring along molecular gradients representing the patterned expression of
709 morphogens and transcription factors (Sansom and Livesey, 2009; Cadwell et al.,
710 2019), which were found to radiate along the rostrocaudal, dorsoventral, and

mediolateral axes of the neural compartment (Hoch et al., 2009). These patterns are conserved to maturity (Vogel et al., 2024) and are consistent with our global connectopies, suggesting a relatively conserved role of genetic profiles in shaping brain organization. Meanwhile, we are proposing an immediate goal to explore the structural connectional basis underlying shifts in macroscale functional organization during development (Dong et al., 2021; Dong et al., 2024).

Another verification warranted in future work is the conservation or changes of global connectopies across species, as the phylogenetically conserved spatiomolecular gradients resemble the similar pattern of genetically encoded signaling pathways and macrostructural organization in various species (Valk et al., 2020; Vogel et al., 2024). A consistent phenomenon of structural connectivity organization across species would provide supporting evidence for overall neuroanatomical similarity, suggesting a basic organizing principle within genetic and connectivity profiles throughout evolution. This is of great significance to the deep exploration of neurodevelopment in humans and non-human animals, which could be integrated into the characterization of genetic and connectional topological patterns at the macro level.

Under the effect of morphogens secreted in the patterning centers with absolute positional information, numerous transcription factors are expressed in a graded manner. For example, the anterior expression of *FGF8* suppresses the posteriorly expressed transcription factors, resulting in their lower anterior but higher posterior expression (Storm et al., 2006). Similarly, manipulation of *EMX2* by genetic knockout

resulted in higher expression posteromedially and lower expression anterolaterally, which caused an expansion of the frontal and lateral regions at the expense of the visual cortex in mice (Hamasaki et al., 2004). These transcription factors are believed to determine the areal fate and expression of cell-surface molecules, thus determining the topographic organization of synaptic inputs and outputs (Rubenstein and Rakic, 1999; Chen et al., 2013) and directing axonal outgrowth (Chilton, 2006). They significantly overlapped with the genes related to the identified global connectopies, which exhibited distinct developmental patterns and especially enriched in radial glial cells in the prenatal period. According to the radial unit hypothesis of cortical development, radial glial cells in the embryonic brain facilitate the generation, placement, and allocation of neurons in the cortex and regulate how they wire up, by acting as a "highway" for axons to facilitate growth and ensuring proper trajectories (Nowakowski et al., 2016; Casingal et al., 2022), during which complex molecular interactions between axons and recipient cortical areas may be involved (Kast and Levitt, 2019).

Exploration of the white matter associated with the global connectopies is marked by the important influences exerted by older brain structures in cortical development and arealization. The thalamo- and striato-cortical projections contributed to the formation of structural organization patterns, especially the first principal component, which varied along the same axis as the functionally distinct dorsal-ventral systems that evolved from two primordial brain structures, following the dual origin theory (Giaccio, 2006; Pandya et al., 2015). As an important mediator of

sensory experience, the thalamus accelerates initial synaptic plasticity and forms direct topographic projections to cortical areas during development, thus influencing regional differentiation of the neocortex (Molnar and Blakemore, 1995; Park et al., 2024). Moreover, another early brain structure, the brainstem, sends ascending neural projections to the developing cortex and also routes sensory input to corresponding brain areas, helping shape anatomical development (Fritzsch et al., 2022). The brainstem houses key neuromodulatory systems, including the noradrenergic, serotonergic, and dopaminergic systems. These systems play a crucial role in influencing cortical plasticity and connectivity. Ultimately, they contribute to the functional differentiation of cortical areas (Taylor et al., 2022; Shine, 2023).

Several technical and methodological limitations must be acknowledged in the current work. The first and most direct concern is the accuracy of mapping structural connections using diffusion tensor imaging. However, diffusion tractography has been used as an irreplaceable tool to identify white matter across the brain in vivo and non-invasively, with certain limitations imposed by the tractography which can cause false positive results (Maier-Hein et al., 2017). In the future, joint MRI and microscopy data analysis may help address these limitations (Huang et al., 2021; Axer and Amunts, 2022; Howard et al., 2023). Distance and geometry effects also need to be considered when mapping the structural connectivity pattern. Still, the consistency between genetic topography and global connectopies suggests that our findings are not simply due to spatial autocorrelation. Although the association

between cortical geometry and brain function should be recognized (Pang et al., 2023), the interaction of structural connectivity and cortical geometry deserves further attention to reveal the function realization of the developing human brain, especially the neonate brain (Dubois et al., 2014). The underlying genetic drivers should also be considered to explore the causal relationship between them by animal studies, which will reduce the impact of mismatch of ages and other factors resulting from relating HCP young adult diffusion MRI connectopies to AHBA-based gene expression information. Although the AHBA is the densest sample transcriptomic dataset of the human brain to date, it comes with the limitations mentioned above, as well as the gap between post-mortem changes in gene expression level and in vivo features, making our results a matter of caution. With the development of RNA sequencing technology, which enables rapid profiling and deep investigation of the transcriptome, more genes could be detected and provide valuable information (Wang et al., 2009). In addition, the observed organizing principles in the current work may also be used to guide the engineering of three-dimensional cortical spheroids and to comprehend the human-specific aspects of the neural circuit assembly (Sloan et al., 2018; Miura et al., 2022).

To conclude, we explored how genes link the accurate formation of connections despite significant differences in their numbers. Our findings revealed the existence of a low-dimensional, topological representation of brain connectivity that may share a common space with gene expression, providing a consistent characterization of

cortical arealization. We hope our discoveries will offer valuable insights into studying brain structure and function.

Data availability

Data from the Human Connectome Project can be downloaded at https://db.humanconnectome.org/. Data from the Chinese Human Connectome Project can be downloaded at https://www.Chinese-HCP.cn. The human gene expression data are available in the Allen Brain Atlas (https://human.brain-map.org/static/download). Data from BrainSpan can be downloaded at https://www.brainspan.org/.

Code availability

The HCP pipeline can be found at https://github.com/Washington-University/HCPpipelines. The neuroimaging preprocessing software used for the other datasets is freely available (FreeSurfer v6.0, http://surfer.nmr.mgh.harvard.edu/, and FSL v6.0.5, https://fsl.fmrib.ox.ac.uk/fsl/fslwiki). The gene processing pipeline is available (abagen, https://github.com/rmarkello/abagen), and gene enrichment analysis is conducted at https://toppgene.cchmc.org/. The cell-type enrichment analysis process was conducted at http://www.cellgo.world. The brain maps were presented using BrainSpace (https://brainspace.readthedocs.io/) and Connectome Workbench v1.5.0 (https://www.humanconnectome.org/software/connectome-workbench). The tracts were visualized using BrainNet Viewer v1.7 (https://www.nitrc.org/projects/bnv/).

Python code to reproduce the analyses and figures is available at

https://github.com/FANLabCASIA/GC.git (will make this public upon acceptance).

References

Adra CN, Iyengar AR, Syed FA, Kanaan IN, Rilo HL, Yu W, Kheraj R, Lin SR, Horiuchi T, Khan S, Weremowicz S, Lim B, Morton CC, Higgs DR (1998) Human ARHGDIG, a GDP-dissociation inhibitor for Rho proteins: genomic structure, sequence, expression analysis, and mapping to chromosome 16p13.3. Genomics 53:104-109.

Arikkath J (2012) Molecular mechanisms of dendrite morphogenesis. Front Cell Neurosci 6:61.

Arnatkeviciute A, Fulcher BD, Fornito A (2019) A practical guide to linking brain-wide gene expression and neuroimaging data. Neuroimage 189:353-367.

Atasoy S, Donnelly I, Pearson J (2016) Human brain networks function in connectome-specific harmonic waves. Nat Commun 7:10340.

Axer M, Amunts K (2022) Scale matters: The nested human connectome. Science 378:500-504.

Behrens TE, Berg HJ, Jbabdi S, Rushworth MF, Woolrich MW (2007) Probabilistic diffusion tractography with multiple fibre orientations: What can we gain? Neuroimage 34:144-155.

Burt JB, Demirtas M, Eckner WJ, Navejar NM, Ji JL, Martin WJ, Bernacchia A, Anticevic A, Murray JD (2018) Hierarchy of transcriptomic specialization across human cortex captured by structural neuroimaging topography. Nat Neurosci 21:1251-1259.

Cadwell CR, Bhaduri A, Mostajo-Radji MA, Keefe MG, Nowakowski TJ (2019) Development and Arealization of the Cerebral Cortex. Neuron 103:980-1004.

Casingal CR, Descant KD, Anton ES (2022) Coordinating cerebral cortical construction and connectivity: Unifying influence of radial progenitors. Neuron 110:1100-1115.

Chen CH, Panizzon MS, Eyler LT, Jernigan TL, Thompson W, Fennema-Notestine C, Jak AJ, Neale MC, Franz CE, Hamza S, Lyons MJ, Grant MD, Fischl B, Seidman LJ, Tsuang MT, Kremen WS, Dale AM (2011) Genetic influences on cortical regionalization in the human brain. Neuron 72:537-544.

Chen CH, Gutierrez ED, Thompson W, Panizzon MS, Jernigan TL, Eyler LT, Fennema-Notestine C, Jak AJ, Neale MC, Franz CE, Lyons MJ, Grant MD, Fischl B, Seidman LJ, Tsuang MT, Kremen WS, Dale AM (2012) Hierarchical genetic organization of human cortical surface area. Science 335:1634-1636.

Chen CH, Fiecas M, Gutierrez ED, Panizzon MS, Eyler LT, Vuoksimaa E, Thompson WK, Fennema-Notestine C, Hagler DJ, Jr., Jernigan TL, Neale MC, Franz CE, Lyons MJ, Fischl B, Tsuang MT, Dale AM, Kremen WS (2013) Genetic topography of brain morphology. Proc Natl Acad Sci U S A 110:17089-17094.

Cheng L, Zhang Y, Li G, Wang J, Sherwood C, Gong G, Fan L, Jiang T (2021) Connectional asymmetry of the inferior parietal lobule shapes hemispheric specialization in humans, chimpanzees, and rhesus macaques. Elife 10.

Chilton JK (2006) Molecular mechanisms of axon guidance. Dev Biol 292:13-24.

Chu C, Li W, Shi W, Wang H, Wang J, Liu Y, Liu B, Elmenhorst D, Eickhoff SB, Fan L, Jiang T (2024) Co-representation of Functional Brain Networks Is Shaped by Cortical Myeloarchitecture and Reveals Individual Behavioral Ability. J Neurosci 44.

Coifman RR, Lafon SJA, analysis ch (2006) Diffusion maps. 21:5-30.

Cui Y, Liu B, Zhou Y, Fan L, Li J, Zhang Y, Wu H, Hou B, Wang C, Zheng F, Qiu C, Rao LL, Ning Y, Li S, Jiang T (2016) Genetic Effects on Fine-Grained Human Cortical Regionalization. Cereb Cortex 26:3732-3743.

Cui Z et al. (2020) Optimization of energy state transition trajectory supports the development of executive function during youth. Elife 9.

Dong HM, Margulies DS, Zuo XN, Holmes AJ (2021) Shifting gradients of macroscale cortical organization mark the transition from childhood to adolescence. Proc Natl Acad Sci U S A 118.

Dong HM, Zhang XH, Labache L, Zhang S, Ooi LQR, Yeo BTT, Margulies DS, Holmes AJ, Zuo XN (2024) Ventral attention network connectivity is linked to cortical maturation and cognitive ability in childhood. Nat Neurosci 27:2009-2020.

Dubois J, Dehaene-Lambertz G, Kulikova S, Poupon C, Huppi PS, Hertz-Pannier L (2014) The early development of brain white matter: a review of imaging studies in fetuses, newborns and infants. Neuroscience 276:48-71.

Fan L (2021) Mapping the Human Brain: What Is the Next Frontier? Innovation (Camb) 2:100073.

Fan L, Li H, Zhuo J, Zhang Y, Wang J, Chen L, Yang Z, Chu C, Xie S, Laird AR, Fox PT, Eickhoff SB, Yu C, Jiang T (2016) The Human Brainnetome Atlas: A New Brain Atlas Based on Connectional Architecture. Cereb Cortex 26:3508-3526.

Fan X, Fu Y, Zhou X, Sun L, Yang M, Wang M, Chen R, Wu Q, Yong J, Dong J, Wen L, Qiao J, Wang X, Tang F (2020) Single-cell transcriptome analysis reveals cell lineage specification in temporal-spatial patterns in human cortical development. Sci Adv 6:eaaz2978.

Fjell AM, Chen CH, Sederevicius D, Sneve MH, Grydeland H, Krogsrud SK, Amlien I, Ferschmann L, Ness H, Folvik L, Beck D, Mowinckel AM, Tamnes CK, Westerhausen R, Haberg AK, Dale AM, Walhovd KB (2019) Continuity and Discontinuity in Human Cortical Development and Change From Embryonic Stages to Old Age. Cereb Cortex 29:3879-3890.

Flores-Sarnat L, Sarnat HB (2008) Axes and gradients of the neural tube for a morphological/molecular genetic classification of nervous system malformations. Handb Clin Neurol 87:1-11.

Fritzsch B, Elliott KL, Yamoah EN (2022) Neurosensory development of the four brainstem-projecting sensory systems and their integration in the telencephalon. Front Neural Circuits 16:913480.

Ge J, Yang G, Han M, Zhou S, Men W, Qin L, Lyu B, Li H, Wang H, Rao H, Cui Z, Liu H, Zuo XN, Gao JH (2023) Increasing diversity in connectomics with the Chinese Human Connectome Project. Nat Neurosci 26:163-172.

Giaccio RG (2006) The dual origin hypothesis: an evolutionary brain-behavior framework for analyzing psychiatric disorders. Neurosci Biobehav Rev 30:526-550.

Glasser MF, Sotiropoulos SN, Wilson JA, Coalson TS, Fischl B, Andersson JL, Xu J, Jbabdi S, Webster M, Polimeni JR, Van Essen DC, Jenkinson M, Consortium WU-MH (2013) The minimal preprocessing pipelines for the Human Connectome Project. Neuroimage 80:105-124.

Gordon EM, Laumann TO, Adeyemo B, Huckins JF, Kelley WM, Petersen SE (2016) Generation and Evaluation of a Cortical Area Parcellation from Resting-State Correlations. Cereb Cortex 26:288-303.

Greig LC, Woodworth MB, Galazo MJ, Padmanabhan H, Macklis JD (2013) Molecular logic of neocortical projection neuron specification, development and diversity. Nat Rev Neurosci 14:755-769.

Gu S, Pasqualetti F, Cieslak M, Telesford QK, Yu AB, Kahn AE, Medaglia JD, Vettel JM, Miller MB, Grafton ST, Bassett DS (2015) Controllability of structural brain networks. Nat Commun 6:8414.

Hamasaki T, Leingartner A, Ringstedt T, O'Leary DD (2004) EMX2 regulates sizes and positioning of the primary sensory and motor areas in neocortex by direct specification of cortical progenitors. Neuron 43:359-372.

Hassan BA, Hiesinger PR (2015) Beyond Molecular Codes: Simple Rules to Wire Complex Brains. Cell 163:285-291.

Hawrylycz M et al. (2015) Canonical genetic signatures of the adult human brain. Nat Neurosci 18:1832-1844.

Hendee K, Wang LW, Reis LM, Rice GM, Apte SS, Semina EV (2017) Identification and functional analysis of an ADAMTSL1 variant associated with a complex phenotype including congenital glaucoma, craniofacial, and other systemic features in a three-generation human pedigree. Hum Mutat 38:1485-1490.

Hernandez-Fernandez M, Reguly I, Jbabdi S, Giles M, Smith S, Sotiropoulos SN (2019) Using GPUs to accelerate computational diffusion MRI: From microstructure estimation to tractography and connectomes. Neuroimage 188:598-615.

Heyen CA, Tagliabracci VS, Zhai L, Roach PJ (2009) Characterization of mouse UDP-glucose pyrophosphatase, a Nudix hydrolase encoded by the Nudt14 gene. Biochem Biophys Res Commun 390:1414-1418.

Hoch RV, Rubenstein JL, Pleasure S (2009) Genes and signaling events that establish regional patterning of the mammalian forebrain. Semin Cell Dev Biol 20:378-386.

Howard AFD, Huszar IN, Smart A, Cottaar M, Daubney G, Hanayik T, Khrapitchev AA, Mars RB, Mollink J, Scott C, Sibson NR, Sallet J, Jbabdi S, Miller KL (2023) An open resource combining multi-contrast MRI and microscopy in the macaque brain. Nat Commun 14:4320.

Huang SY et al. (2021) Connectome 2.0: Developing the next-generation ultra-high gradient strength human MRI scanner for bridging studies of the micro-, meso- and macro-connectome. Neuroimage 243:118530.

Huang Y, Wu Z, Li T, Wang X, Wang Y, Xing L, Zhu H, Lin W, Wang L, Guo L, Gilmore JH, Li G (2023) Mapping Genetic Topography of Cortical Thickness and Surface Area in Neonatal Brains. J Neurosci.

Huntenburg JM, Bazin PL, Margulies DS (2018) Large-Scale Gradients in Human Cortical Organization. Trends Cogn Sci 22:21-31.

Janelle F, Iorio-Morin C, D'Amour S, Fortin D (2022) Superior Longitudinal Fasciculus: A Review of the Anatomical Descriptions With Functional Correlates. Front Neurol 13:794618.

Kast RJ, Levitt P (2019) Precision in the development of neocortical architecture: From progenitors to cortical networks. Prog Neurobiol 175:77-95.

Krenke K, Szczaluba K, Bielecka T, Rydzanicz M, Lange J, Koppolu A, Ploski R (2019) FARSA mutations mimic phenylalanyl-tRNA synthetase deficiency caused by FARSB defects. Clin Genet 96:468-472.

Langen M, Agi E, Altschuler DJ, Wu LF, Altschuler SJ, Hiesinger PR (2015) The Developmental Rules of Neural Superposition in Drosophila. Cell 162:120-133.

Li P, Wei J, Zhu Y (2023) CellGO: a novel deep learning-based framework and webserver for cell-type-specific gene function interpretation. Brief Bioinform 25.

Lu S, Hernan R, Marcogliese PC, Huang Y, Gertler TS, Akcaboy M, Liu S, Chung HL, Pan X, Sun X, Oguz MM, Oztoprak U, de Baaij JHF, Ivanisevic J, McGinnis E, Guillen Sacoto MJ, Chung WK, Bellen HJ (2022) Loss-of-function variants in TIAM1 are associated with developmental delay, intellectual disability, and seizures. Am J Hum Genet 109:571-586.

Ma S et al. (2022) Molecular and cellular evolution of the primate dorsolateral prefrontal cortex. Science 377:eabo7257.

Maier-Hein KH et al. (2017) The challenge of mapping the human connectome based on diffusion tractography. Nat Commun 8:1349.

Mansour LS, Tian Y, Yeo BTT, Cropley V, Zalesky A (2021) High-resolution connectomic fingerprints: Mapping neural identity and behavior. Neuroimage 229:117695.

Margulies DS, Ghosh SS, Goulas A, Falkiewicz M, Huntenburg JM, Langs G, Bezgin G, Eickhoff SB, Castellanos FX, Petrides M, Jefferies E, Smallwood J (2016) Situating the default-mode network along a principal gradient of macroscale cortical organization. Proc Natl Acad Sci U S A 113:12574-12579.

Markello RD, Arnatkeviciute A, Poline JB, Fulcher BD, Fornito A, Misic B (2021) Standardizing workflows in imaging transcriptomics with the abagen toolbox. Elife 10.

Mars RB, Sotiropoulos SN, Passingham RE, Sallet J, Verhagen L, Khrapitchev AA, Sibson N, Jbabdi S (2018) Whole brain comparative anatomy using connectivity blueprints. Elife 7.

Miller JA et al. (2014) Transcriptional landscape of the prenatal human brain. Nature 508:199-206.

Miura Y, Li MY, Revah O, Yoon SJ, Narazaki G, Pasca SP (2022) Engineering brain assembloids to interrogate human neural circuits. Nat Protoc 17:15-35.

Molnar Z, Blakemore C (1995) How do thalamic axons find their way to the cortex? Trends Neurosci 18:389-397.

Molnar Z, Clowry GJ, Sestan N, Alzu'bi A, Bakken T, Hevner RF, Huppi PS, Kostovic I, Rakic P, Anton ES, Edwards D, Garcez P, Hoerder-Suabedissen A, Kriegstein A (2019) New insights into the development of the human cerebral cortex. J Anat 235:432-451.

Morgan SE, Seidlitz J, Whitaker KJ, Romero-Garcia R, Clifton NE, Scarpazza C, van Amelsvoort T, Marcelis M, van Os J, Donohoe G, Mothersill D, Corvin A, Pocklington A, Raznahan A, McGuire P, Vertes PE, Bullmore ET (2019) Cortical patterning of abnormal morphometric similarity in psychosis is associated with brain expression of schizophrenia-related genes. Proc Natl Acad Sci U S A 116:9604-9609.

Neale MC, Hunter MD, Pritikin JN, Zahery M, Brick TR, Kirkpatrick RM, Estabrook R, Bates TC, Maes HH, Boker SM (2016) OpenMx 2.0: Extended Structural Equation and Statistical Modeling. Psychometrika 81:535-549.

Nowakowski TJ, Pollen AA, Sandoval-Espinosa C, Kriegstein AR (2016) Transformation of the Radial Glia Scaffold Demarcates Two Stages of Human Cerebral Cortex Development. Neuron 91:1219-1227.

O'Leary DD, Sahara S (2008) Genetic regulation of arealization of the neocortex. Curr Opin Neurobiol 18:90-100.

Pandya D, Seltzer B, Petrides M, Cipolloni PB (2015) Cerebral Cortex: Architecture, Connections, and the Dual Origin Concept: Oxford University Press.

Pang JC, Aquino KM, Oldehinkel M, Robinson PA, Fulcher BD, Breakspear M, Fornito A (2023) Geometric constraints on human brain function. Nature 618:566-574.

Paquola C, Vos De Wael R, Wagstyl K, Bethlehem RAI, Hong SJ, Seidlitz J, Bullmore ET, Evans AC, Misic B, Margulies DS, Smallwood J, Bernhardt BC (2019) Microstructural and functional gradients are increasingly dissociated in transmodal cortices. PLoS Biol 17:e3000284.

Park S, Haak KV, Oldham S, Cho H, Byeon K, Park BY, Thomson P, Chen H, Gao W, Xu T, Valk S, Milham MP, Bernhardt B, Di Martino A, Hong SJ (2024) A shifting role of thalamocortical connectivity in the emergence of cortical functional organization. Nat Neurosci 27:1609-1619.

Passingham RE, Stephan KE, Kotter R (2002) The anatomical basis of functional localization in the cortex. Nat Rev Neurosci 3:606-616.

Preti MG, Van De Ville D (2019) Decoupling of brain function from structure reveals regional behavioral specialization in humans. Nat Commun 10:4747.

Rakic P, Ayoub AE, Breunig JJ, Dominguez MH (2009) Decision by division: making cortical maps. Trends Neurosci 32:291-301.

Robinson EC, Jbabdi S, Glasser MF, Andersson J, Burgess GC, Harms MP, Smith SM, Van Essen DC, Jenkinson M (2014) MSM: a new flexible framework for Multimodal Surface Matching. Neuroimage 100:414-426.

Robinson PA, Zhao X, Aquino KM, Griffiths JD, Sarkar S, Mehta-Pandejee G (2016) Eigenmodes of brain activity: Neural field theory predictions and comparison with experiment. Neuroimage 142:79-98.

Ru Q, Lu Y, Saifullah AB, Blanco FA, Yao C, Cata JP, Li DP, Tolias KF, Li L (2022) TIAM1-mediated synaptic plasticity underlies comorbid depression-like and ketamine antidepressant-like actions in chronic pain. J Clin Invest 132.

Rubenstein JL, Rakic P (1999) Genetic control of cortical development. Cereb Cortex 9:521-523.

Sansom SN, Livesey FJ (2009) Gradients in the brain: the control of the development of form and function in the cerebral cortex. Cold Spring Harb Perspect Biol 1:a002519.

Sansregret L, Nepveu A (2008) The multiple roles of CUX1: insights from mouse models and cell-based assays. Gene 412:84-94.

Schaefer A, Kong R, Gordon EM, Laumann TO, Zuo XN, Holmes AJ, Eickhoff SB, Yeo BTT (2018) Local-Global Parcellation of the Human Cerebral Cortex from Intrinsic Functional Connectivity MRI. Cereb Cortex 28:3095-3114.

Shen EH, Overly CC, Jones AR (2012) The Allen Human Brain Atlas: comprehensive gene expression mapping of the human brain. Trends Neurosci 35:711-714.

Shine JM (2023) Neuromodulatory control of complex adaptive dynamics in the brain. Interface Focus 13:20220079.

Sloan SA, Andersen J, Pasca AM, Birey F, Pasca SP (2018) Generation and assembly of human brain region-specific three-dimensional cultures. Nat Protoc 13:2062-2085.

Srinivasan K, Leone DP, Bateson RK, Dobreva G, Kohwi Y, Kohwi-Shigematsu T, Grosschedl R, McConnell SK (2012) A network of genetic repression and derepression specifies projection fates in the developing neocortex. Proc Natl Acad Sci U S A 109:19071-19078.

Storm EE, Garel S, Borello U, Hebert JM, Martinez S, McConnell SK, Martin GR, Rubenstein JL (2006) Dose-dependent functions of Fgf8 in regulating telencephalic patterning centers. Development 133:1831-1844.

Strick PL (1986) The organization of thalamic inputs to the "premotor" areas. Prog Brain Res 64:99-109.

Takahashi E, Folkerth RD, Galaburda AM, Grant PE (2012) Emerging cerebral connectivity in the human fetal brain: an MR tractography study. Cereb Cortex 22:455-464.

Talozzi L, Forkel SJ, Pacella V, Nozais V, Allart E, Piscicelli C, Perennou D, Tranel D, Boes A, Corbetta M, Nachev P, Thiebaut de Schotten M (2023) Latent disconnectome prediction of long-term cognitive-behavioural symptoms in stroke. Brain 146:1963-1978.

Tarun A, Behjat H, Bolton T, Abramian D, Van De Ville D (2020) Structural mediation of human brain activity revealed by white-matter interpolation of fMRI. Neuroimage 213:116718.

Taylor NL, D'Souza A, Munn BR, Lv J, Zaborszky L, Muller EJ, Wainstein G, Calamante F, Shine JM (2022) Structural connections between the noradrenergic and cholinergic system shape the dynamics of functional brain networks. Neuroimage 260:119455.

Taylor PN, Wang Y, Kaiser M (2017) Within brain area tractography suggests local modularity using high resolution connectomics. Sci Rep 7:39859.

Thiebaut de Schotten M, Foulon C, Nachev P (2020) Brain disconnections link structural connectivity with function and behaviour. Nat Commun 11:5094.

Valk SL, Xu T, Margulies DS, Masouleh SK, Paquola C, Goulas A, Kochunov P, Smallwood J, Yeo BTT, Bernhardt BC, Eickhoff SB (2020) Shaping brain structure: Genetic and phylogenetic axes of macroscale organization of cortical thickness. Sci Adv 6.

Van Essen DC, Smith SM, Barch DM, Behrens TE, Yacoub E, Ugurbil K, Consortium WU-MH (2013) The WU-Minn Human Connectome Project: an overview. Neuroimage 80:62-79.

Van Haastert PJ, Devreotes PN (2004) Chemotaxis: signalling the way forward. Nat Rev Mol Cell Biol 5:626-634.

Vogel JW, Alexander-Bloch AF, Wagstyl K, Bertolero MA, Markello RD, Pines A, Sydnor VJ, Diaz-Papkovich A, Hansen JY, Evans AC, Bernhardt B, Misic B, Satterthwaite TD, Seidlitz J (2024) Deciphering the functional specialization of whole-

brain spatiomolecular gradients in the adult brain. Proc Natl Acad Sci U S A 121:e2219137121.

Wang Y, Wang Y, Wang H, Ma L, Eickhoff SB, Madsen KH, Chu C, Fan L (2024) Spatio-molecular profiles shape the human cerebellar hierarchy along the sensorimotor-association axis. Cell Rep 43:113770.

Wang Z, Gerstein M, Snyder M (2009) RNA-Seq: a revolutionary tool for transcriptomics. Nat Rev Genet 10:57-63.

Wasserthal J, Neher P, Maier-Hein KH (2018) TractSeg - Fast and accurate white matter tract segmentation. Neuroimage 183:239-253.

Wu D (2005) Signaling mechanisms for regulation of chemotaxis. Cell Res 15:52-56.

Yang F, De La Fuente R, Leu NA, Baumann C, McLaughlin KJ, Wang PJ (2006) Mouse SYCP2 is required for synaptonemal complex assembly and chromosomal synapsis during male meiosis. J Cell Biol 173:497-507.

Zhu P, Zhou W, Wang J, Puc J, Ohgi KA, Erdjument-Bromage H, Tempst P, Glass CK, Rosenfeld MG (2007) A histone H2A deubiquitinase complex coordinating histone acetylation and H1 dissociation in transcriptional regulation. Mol Cell 27:609-621.

Figures

Figure 1. Overview of the analysis pipeline. We investigated the hypothesis that the existence of a common space is shared by brain connectivity and genetic profiles. (a) The construction of global connectopies (GCs). White matter tractograms were calculated to generate a similarity matrix, i.e., a tractogram covariance (TC) matrix. Diffusion map embedding was implemented on the TC matrix, resulting in low-dimensional gradients. **(b)** Biological interpretation of the GCs. White matter bundles contributing to the GCs were analyzed (top panel). Global connectopies were demonstrated to provide a large-scale descriptor of cortical cartography, which may give insight into cortical parcellation (Fan et al., 2016). **(c)** Topographic axes of genetic profiles. We demonstrated a correspondence between the genetic influence on cortical morphology and global connectopies. We established that the three global connectopies are consistent with morphogen gradients in the developing brain and spatiomolecular gradients in adulthood and provided evidence that specific genes drive the formation of the cortical organization. **(d)** Annotation of GCs-associated genes. Genes associated with the GCs were identified and submitted to enrichment and development analyses.

Figure 2. The three global connectopies and the white matter tracts contribute to the GCs. (a) The first three global connectopies run dorsoventrally, rostrocaudally, and mediolaterally and are termed GC1-DV, GC2-RC, and GC3-ML, respectively. These patterns are stable along subjects (Figure 2-1) and are not affected by age, sex, or brain size (Figure 2-2). An independent experience was also applied on

CHCP dataset (Figure 2-3). Moreover, these three patterns are highly reproducible between individuals (Figure 2-4), and can be reproduced in ROI-wise (Figure 2-5). The GCs are beyond geodesic distance and cortical geometry (Figure S2-6, 2-7) and demonstrated the role of long-range connections in the formation of global connectopies (Figure 2-8). **(b)** The three global connectopies are projected onto the white matter (Figure 2-9), and are situated by distinct sets of white matter tracts. The white matter tracts were reconstructed by TractSeg (Table 2-1). Mean values and variances of the contributions of five types of tracts to the global connectopies are shown. The numerical values are showed in Figure 2-10. Each dot represents one tract. Different colors represent different types of tracts, with deeper colors indicating higher contributions. The two right columns show two types of characteristic tracts contributing to the global connectopies, with one type of tract situated at one extreme of the global connectopy while the other stretching across the global connectopy. The first column shows the cortical projection on the surface of the tract, and the second shows the corresponding fiber bundles reconstructed by TractSeg. See Table 2-1 and Figure 2-1to Figure 2-10 for more details.

Figure 3. Global connectopies provide a large-scale descriptor of arealization. **(a)** The three global connectopies were plotted together in what we termed the global connectopic space, with connectopy values assigned to the RGB values at each vertex. The global connectopic space integrates the information of the three global connectopies and quantifies the topography of the dominant global connectopy. **(b)** Left: Several lobes or subregions clearly appear when every two global connectopies

are plotted together in 2D space, with the extremes of the GCs clearly and continuously shown. GC1-DV and GC2-RC split the cortex into the prefrontal cortex and limbic cortex, sensorimotor cortex, and occipitotemporal cortex. GC1-DV and GC3-ML split the cortex into the frontal cortex, limbic cortex, and occipitotemporal cortex. GC2-RC and GC3-ML split the cortex into the prefrontal cortex, limbic cortex, and other regions. Right: The three GCs were plotted together in 3D space. Vertices were assigned different colors according to the signs of the three axes. **(c)** Modules identified by hierarchical clustering using the three global connectopies. At each level, the brain was partitioned into two modules according to the positive and negative signs of the global connectopy. Eight modules, including lobes or functional networks, emerged clearly. vSomaMot ventral somatomotor cortex, dSomaMot dorsal somatomotor cortex, lPFC lateral prefrontal cortex, CG cingulate gyrus, ITC lateral temporal cortex, AG angular gyrus, mOC medial occipital cortex, OPC occipital polar cortex, OFC orbitofrontal cortex, vmPFC ventromedial prefrontal cortex, PCC posterior cingulate cortex.

Figure 4. Global connectopies correspond to genetic topography. (a) The first three gradients of genetic similarity of cortical thickness. The genetic similarity matrix was calculated by fitting bivariate ACE models to compute the genetic correlations of cortical thickness between two vertices in a twin dataset (Figure 4-1). **(b)** The three gradients of genetic similarity of cortical thickness show a high correlation with global connectopies ($r_{GC1\text{-}DV,\ GG3\text{-}Thickness} = 0.72$, $p_{spin} < .0028$, FDR corrected; $r_{GC2\text{-}RC,\ GG1\text{-}Thickness} = 0.91$, $p_{spin} < .0001$, FDR corrected; $r_{GC3\text{-}ML,\ GG2\text{-}Thickness} = 0.72$, $p_{spin} < .0041$,

FDR corrected). The global connectopies can be replicated by twin data (Figure 4-2). **(c)** Overlap between four modules derived from hierarchical clustering and genetic patterning of cortical thickness. Four-cluster genetic patterning was obtained by performing fuzzy clustering on the genetic similarity matrix, which corresponds to well-known brain regions (Figure 4-3, Figure 4-4). *** $p < .001$, ** $p < .01$, * $p < .05$. See Figure 4-1 to Figure 4-4 for more details.

Figure 5. Consistency between global connectopies and morphogen gradients and spatiomolecular gradients. (a) The expression of morphogen genes which mostly exhibited high differential stability across individuals (Table 5-1) and followed the same pattern as any of the three global connectopies was significantly different between the two ends of the global connectopies (two-sample t-test, all $p < .001$). The number of subdivisions does not affect the final results (Figure 5-1). **(b)** The global connectopies significantly correlated with the spatiomolecular gradients, which maintained the same pattern as morphogenetic gradients during development ($r_{GC1\text{-}DV,\ LV1} = 0.74$, $p_{spin} < .0060$, FDR corrected; $r_{GC2\text{-}RC,\ LV2} = 0.75$, $p_{spin} < .0012$, FDR corrected; $r_{GC3\text{-}ML,\ LV3} = 0.5$, $p_{spin} < .0233$, FDR corrected). *** $p < .001$. See Table 5-1 and Figure 5-1 for more details.

Figure 6. Gene enrichment analysis of connectopy-associated genes. (a) Distributions of connectopic weights across genes. Genes in the top 0.83% of either tail of the distribution ($n = 130$) were selected for further enrichment analysis. The Venn diagram showing the overlap of genes is shown on the right. **(b)** Top genes for unique connectopy and overlap of connectopies. **(c)** Cell type enrichment analysis

was conducted on genes belonging to each GC using prenatal and postnatal datasets. These genes are significantly enriched in radial glial cells in prenatal samples and enriched in excitatory neurons after birth. **(d)** The development spectrum of gene expression for each brain macrostructure. Genes associated with GCs were highly expressed in the prenatal period and decreased after birth. **(e)** Gene set enrichment across all GC-related genes indicated terms related to the regulation of transcription, metabolic process, morphogenesis, cellular development, and neuron projection.

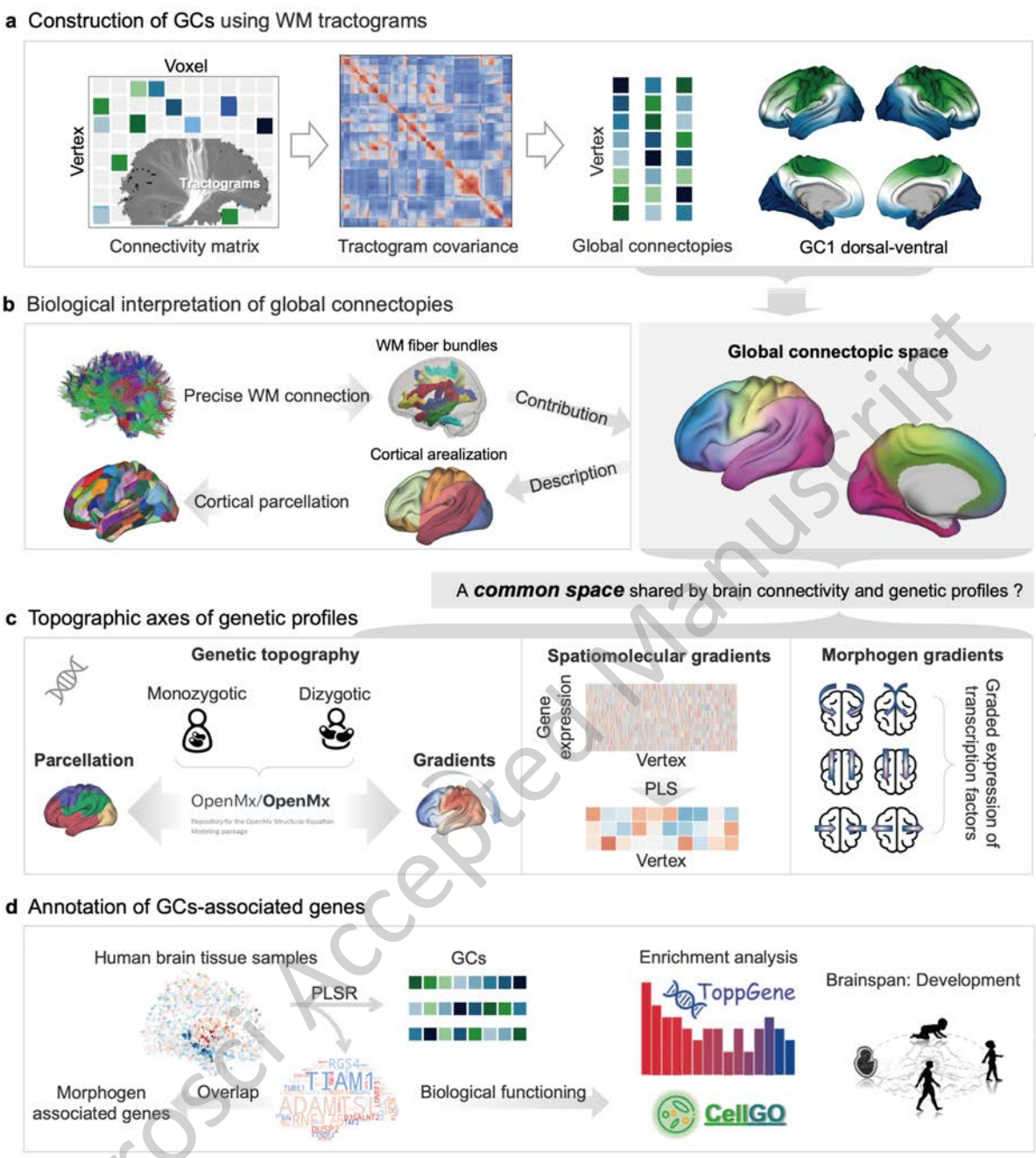

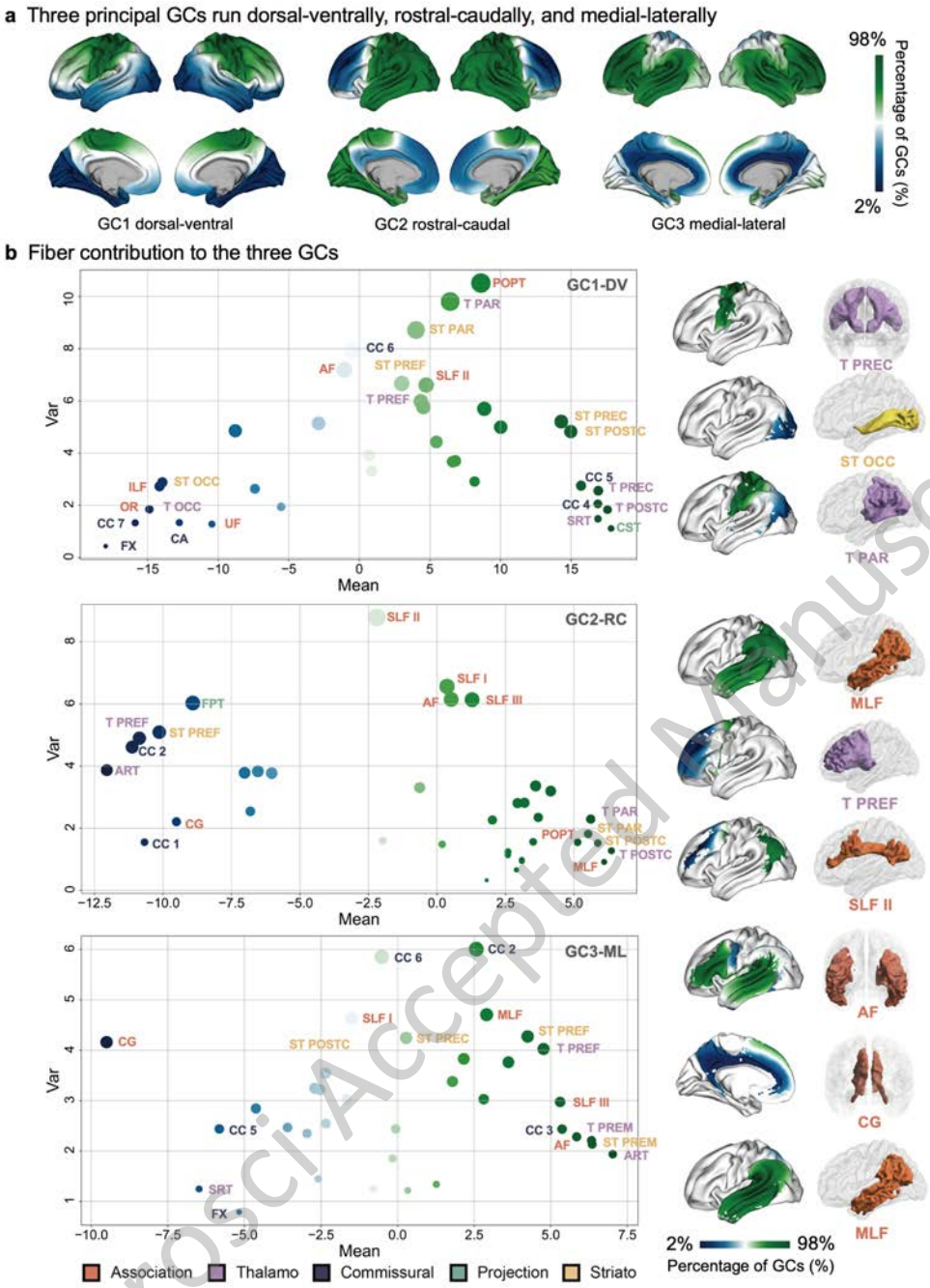

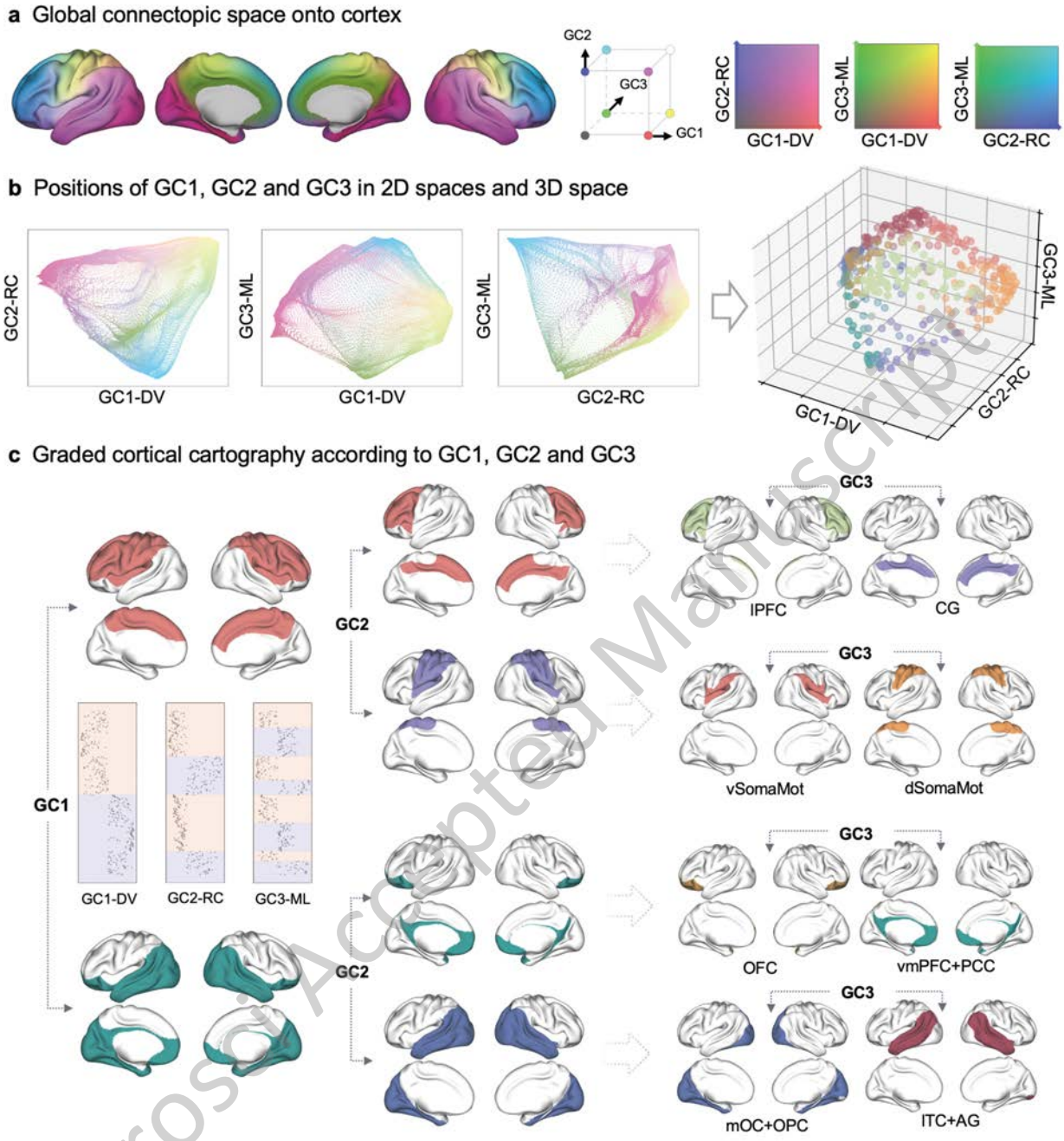

a Genetic gradients pattern of thickness in left hemisphere

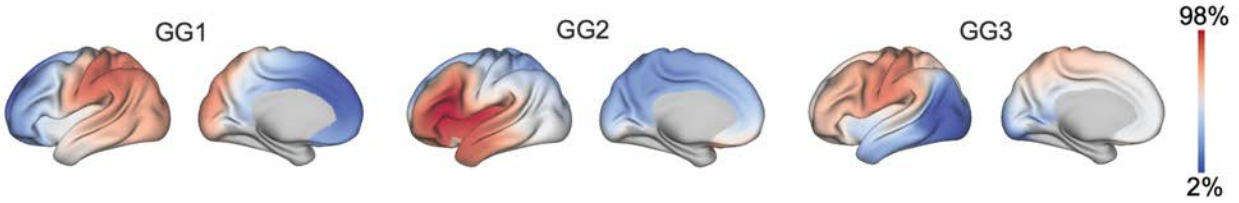

b Genetic gradients of thickness correlate with GCs

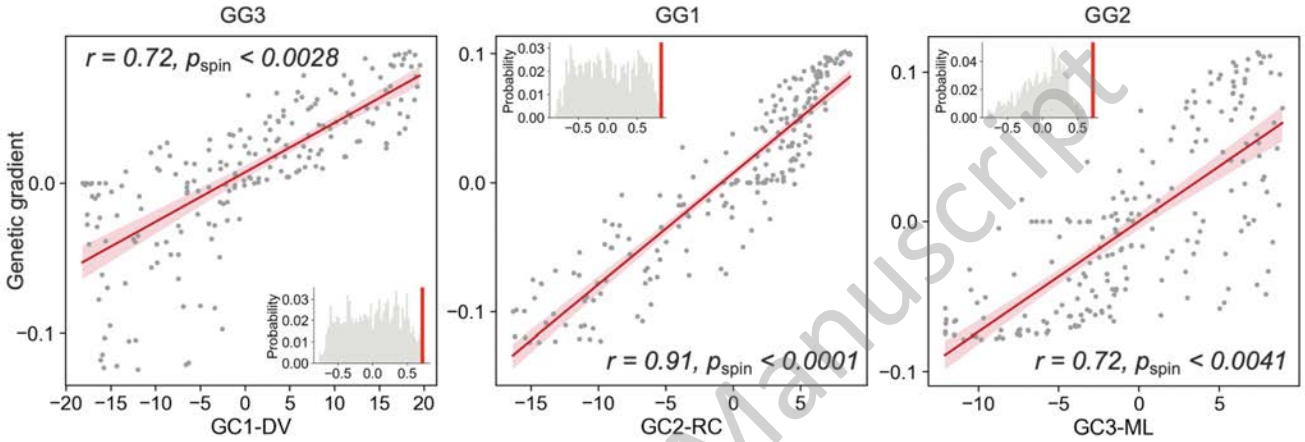

c Overlap between clustering with genetic patterning